SGP-TR-182

Electrical Impedance Tomography

Robert W. Stacey

June 2006

Financial support was provided through the
Stanford Geothermal Program under
Department of Energy Grant No. DE-FG36-02ID14418,
and by the Department of Petroleum Engineering,
Stanford University

Stanford Geothermal Program
Interdisciplinary Research in
Engineering and Earth Sciences
STANFORD UNIVERSITY

Abstract

Three-dimensional Electrical Impedance Tomography (EIT) is a technique that has the potential to provide estimates of reservoir saturation at multiple scales by determining the resistivity distribution within the subsurface. In theory EIT is well suited for researching geothermal systems due to the large contrast in resistivity between the liquid and vapor phases. Here in our initial laboratory investigation we have applied the EIT technique to measure the saturation distribution within a core.

The initial EIT experiment presented here used a Berea sandstone core with 48 electrodes attached in three rings of 16. The core was open to the atmosphere with saturation occurring by natural imbibition and desaturation by evaporation. The voltage potential field was measured by applying a direct current pulse across the core and measuring the voltage potential at all electrodes, essentially applying the 4-wire resistance technique over all electrodes in turn. The result was a data set that embodies the resistivity distribution within the core, and by inversion the resistivity distribution was reconstructed, which allowed for the inference of the saturation.

The data processing was accomplished by utilizing the EIDORS toolkit which was developed for application to this nonlinear and ill-posed inverse problem. The procedure utilizes a finite element model for forward calculation and a regularized nonlinear inverse solver to obtain a unique and stable inverse solution (Polydorides et al. 2002).

Experiments have indicated EIT is a viable technique for studying the displacement characteristics of fluids with contrasting resistivity, and is capable of detecting displacement fronts in near real-time. The current system is also a quantitative technique able to measure saturation distributions accurately between $20\% < S_w < 65\%$. These limitations were imposed due to connate water connections to the electrodes and ion mobility effects caused by the DC voltage source. It is anticipated that the applicability of EIT will increase to $S_w = 100\%$ with the implementation of an AC voltage source.

Acknowledgments

First and foremost I would like to sincerely thank my advisor Roland N. Horne for always tactfully providing direction throughout my research, for inspiring and embracing unique solutions in the laboratory, and for always staying late to engage in worldy affairs on Friday afternoons. My great thanks go out to Kewen Li for his guidance and insight in the laboratory. Then last but not least, the Geothermal group, Egill, Aysegul, Chumei, Nick, Allen, Anson, and Laura, thank you for your support, humor, and helping hand throughout all the research.

This research was conducted with financial support through the Stanford Geothermal Program under Department of Energy Grant No. DE-FG36-02ID14418.

Contents

List of Tables

List of Figures

Chapter 1

1. Introduction

In a geothermal reservoir system it is crucial to know the extent, the energy intensity, and the connectivity of the resource. Understanding the extent and energy intensity are relatively well understood in comparison to the connectivity. There are multiple techniques to investigate the connectivity at various scales. The injection test, temperature logs, spinner tests, mud logs, etc. All of these methods may be classified as “near well tests”, which provide reservoir characteristic from a single confined location constrained by the location of the well. These inferred characteristics are highly dependent upon the fractures intersected by the well bore.

At the field scale where the question of connectivity between wells is of critical importance, injection and production history data may be used to infer connectivity. However, the productivity of a field may be placed in jeopardy by improper placement of an injection well. Therefore, knowing the connectivity of the reservoir early in development would substantially help minimize risk and maximize productivity throughout the life of a reservoir. For this reason Electrical Impedance Tomography (EIT) at the field scale is of particular interest in identifying connective faults and fractures throughout the reservoir.

However, before any large scale investigations may be pursued with EIT, a laboratory scale EIT system has been developed to investigate core scale fluid interactions that are of equal importance to the life of a reservoir. Core experiments may infer the microscale properties that influence the life of the reservoir significantly; primary and secondary porosity and permeability, relative permeability in fractures, and residual saturation

distribution. Residual saturation is of great significance because the life expectancy of a vapor dominated geothermal field is governed primarily by the amount of residual fluid.

Previous studies have investigated the issue of residual water saturation by two means, inference from production history and X-ray CT core studies. Belen and Horne (2000) developed a method to infer the residual in-situ water saturation from field measurements, but the field must be in production for a period of time before being able to estimate the initial residual saturation. To estimate residual saturations in laboratory experiments ferrous core holders are required to replicate reservoir pressures and temperatures. The use of a ferrous core holder eliminates the use of an X-ray CT scan, and for that reason all previous tests have not been at reservoir temperatures and pressures.

Consequently, due to the critical importance of understanding core scale phenomenon and the limitations of the X-ray CT scan, Electrical Impedance Tomography (EIT) has been investigated as a new technique to image fluid distribution.

1.1. Background

The concept of studying the internal properties of a medium by imposing a current, measuring the voltage distribution, and inferring the internal resistivity is not a new idea. The idea of Electrical Resistive Tomography was proposed independently by Henderson and Webster (1978) for medical imaging and by Lytle and Dines (1978) as a geophysical imaging tool (Daily and Ramirez 2000). Since 1978, computational power has increased drastically to allow for large three-dimensional EIT inversions, and computational time has decreased also due to the implementation of better methods of obtaining the inverse solution.

1.2. EIT Theory

The theory behind electrical impedance tomography is that by applying a constant current across a material the voltage distribution resulting on the surface will reflect the internal resistivity distribution. However, intuitively one will understand that multiple resistivity

distributions can produce the same voltage distribution at the surface. Therefore the system is stimulated in multiple manners to constrain the possible resistivity distributions. Figure 1-1 shows a simple EIT diagram with 16 electrodes around the perimeter of a circular medium. In this setup the current, *I*, is applied across a pair of electrodes on opposite sides of the core while the voltage distribution, *Vi*, is measured between each set of neighboring electrodes. After the voltage around the entire perimeter has been measured, the current drive electrodes are rotated to the neighboring electrode, such that they remain opposite, and the voltage at all electrodes is measured once again. This process continues until the 256 sets of voltage measurements are complete.

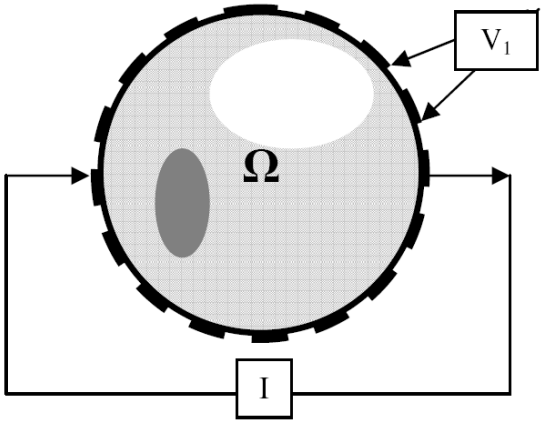

Figure 1-1: EIT Diagram of 16 electrode EIT experiment. The potential V_1 is measured after a current *I* has been imposed across the core Ω. (Molinari 2003)

The governing equation for the voltage field produced by placing a current across a material is shown below in Equation 1.

$$\nabla \cdot (\sigma + \imath\varpi\varepsilon)\nabla\phi = 0 \qquad \textbf{(1)}$$

Where σ is the electric impedance of the medium, ϕ is the electric potential, ϖ is the frequency, and ε is the electric permittivity. Equation 1 is reduced to the standard

governing equation for EIT, Equation 2, when a low frequency or direct current is used, ($\varpi \approx 0$) (Molinari 2003).

$$\nabla \cdot (\sigma \nabla \phi) = 0 \tag{2}$$

The EIT inverse problem is simply a system stimulation problem. The stimulation and resulting effect (injected current *i* and measured voltage *V*) are known, but the internal physical system is unknown (impedance distribution σ). The difficulty in solving this problem is in the nonlinearity that arises in σ, because the potential distribution ϕ is a function of the impedance, $\phi = \phi(\sigma)$, and we cannot easily solve Equation 2 for σ (Molinari 2003). The ill-posed nature of the problem is clearly apparent when observing the diffusive nature of electricity, coupled with inherent measurement errors.

1.3. Previous Studies

1.3.1. Laboratory Studies

Previously there have been multiple studies performed at the laboratory scale, primarily motivated by medical research. While developing EIDORS, (Electrical Impedance Tomography and Diffuse Optical Tomography Reconstruction Software) Polydorides (2002) performed simple EIT experiments on cylinders of water containing metal cylinders. The goal of his experiment was to test and understand the accuracy and applicability of the EIDORS software being developed, and obtained results that reasonably identified an object of high conductivity in the water. Since this time multiple research groups have been working on applying EIT for medical imaging.

The laboratory study that initiated this research project was a paper on imaging flow in a core with EIT by van Weereld (2001). The paper showed that EIT techniques were able to image a two-phase system (oil and brine) at reservoir pressures in near real-time in three dimensions. However, the authors were unable to convert resistivity images to saturation,

or to validate their results against other methods. For this reason it was decided to replicate the experiment, measure saturation, and quantify the results.

1.3.2. Field Studies

Multiple field applications of EIT have been pursued in the area of earth sciences, with some success, but difficulties with measurements and computational inversion persist. ERT has been used to image an injected NaCl tracer in groundwater (Singha and Gorelick 2005) and (Daily and Ramirez 2000), and to detect fractures in a heated rock mass (Roberts et al. 2001).

The experiment by Roberts et al. (2001) is of particular interest due its direct application to geothermal conditions. In this test an excavated 3 m x 3 m x 4.5 m block of rock was heated from ambient conditions to 145ºC with confining pressures up to 100 bar. ERT was able to detect a fracture by observing an area of increased resistivity as the temperature of the block increased. This area of increased resistivity is indicative of the liquid phase in a fractured zone changing to the vapor phase of high resistance. However, the authors were unable to verify the existence of the fracture.

One of the first in-situ ERT tracer experiments was conducted at the Hanford Washington test site by Daily and Ramirez (2000). The experiment consisted of nine wells arranged in a circle 14 m in diameter to a depth of 20 m with 135 electrodes. The authors were able to identify a low resistance anomaly where the tracer was injected and track its progress as it followed the groundwater gradient. However, as in the fracture detection, only coarse bulbous areas of resistance change could be detected. The primary difficulty limiting the data sets resolution was the short-circuiting effect of metal well casings within the site.

A recent ERT tracer experiments was conducted by Singha and Gorelick (2005) in a stratified sand and gravel deposit at the Massachusetts Military Reservation in western Cape Cod. The site consisted of four ERT wells with 24 electrodes each, 33.0 m deep on the sides of a 10 x 14 m area, and contained within the site were the injection, pumping, and multilevel sampling wells. The study was able to quantify the results by comparing

the ERT inferred concentrations to the real concentrations measured by the multilevel sampler. The results indicated that the center of the tracer mass was tracked very well, but only 25% of the tracer mass could be accounted for by ERT.

Chapter 2

2. The EIT System

The EIT system comprises three main areas of development; electrode configuration and connection, data acquisition, and data processing. The latter two areas have been investigated and developed in related fields, particularly the medical field (Polydorides 2002). In this research project the strategy was to investigate how each area had been developed in a related field, and then to transfer the appropriate technique and technology to the core scale application.

2.1. Electrode Configuration and Connection

The electrode connection is one of the greatest difficulties associated with EIT. In several laboratory scale experiments (Van Weereld et al., 2001, Polydorides 2002, and Molinari 2003) it has been found that accurate, consistently geometric connections are difficult to obtain. The electrode material is crucial to the behavior of the system, because each electrode in contact with a salt solution develops an electrochemical interface (Bagotzky 1993). If the electrode material is reversible the chemical reaction can be reversed by reversing the current. If the electrode material is irreversible this is referred to as a polarisable electrode. As examples of each; silver-silver chloride electrodes are nonpolarisable, gold and platinum electrodes are polarisable (Van Weereld et al. 2001). The electrode design decided upon for this experiment was a copper wire loop coated with silver epoxy, Figure 2-1. This design was selected due to the electrodes being nonpolarisable and because of the simple construction and attachment to the core

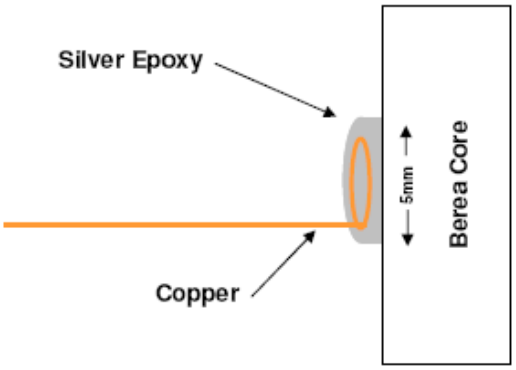

Figure 2-1: Schematic of EIT electrode.

The second consideration is the number and configuration of electrodes on the core. In principle, with more electrodes attached, more independent measurements may be made and the system will be better constrained, resulting in higher confidence and resolution in the inferred resistivity distribution. However, the practical limitations imposed by wiring limits the number that can be attached by hand. Van Weerald's solution to this problem was to use a flexible circuit with 192 electrodes designed specifically for the core. This flexible circuit design ensured consistent size and distribution of electrodes, while also creating a compact manageable system as compared to conventionally wired electrodes (Van Weereld et al. 2001).

Figure 2-2 shows the final design with 3 rings of 16 electrodes attached to the Berea sandstone core with conductive silver epoxy. The core measures 5 cm in diameter and is 10 cm tall. This design was based upon conventional wiring constraints, and Polydorides (2002) suggestion that a 16 electrode ring is the optimum size due to computational time, the noise imposed by additional electrodes, and the fraction of singular values that are useful. The design was also simple enough to reduce or eliminate many foreseen possible future problems, such as system leaks, short circuiting, and poor connections. Yet the system was complex enough with three rings of 16 electrodes to fully test the data acquisition system and the MATLAB toolkit EIDORS in postprocessing. During the

experiment, water imbibed into the core by capillary forces. Therefore, no core holder was required, eliminating the issue of leak problems.

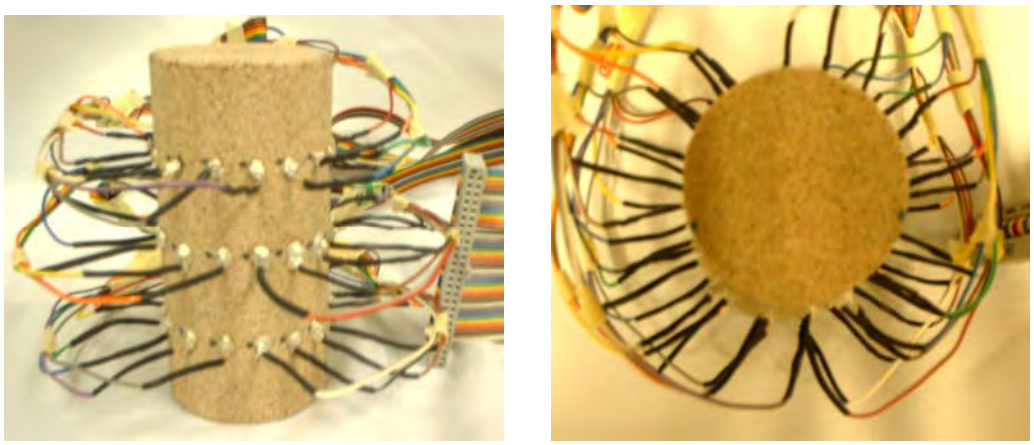

(Side View) (Top View)

Figure 2-2: Side and top view of the electrode design. 48 electrodes were attached to a Berea sandstone core using conductive silver. The core is 5 cm in diameter and 10 cm tall.

2.2. Data Acquisition

The issue of data acquisition has been addressed by several researchers. The Weerled et al. (2001) EIT experiment logged data from 192 electrodes in near real-time. However, the optimum order and procedure in collecting data is not standardized. The procedure has been debated by Molinari (2003) and Polydorides (2002), both of whom have modeled the system at hand extensively, but have published little physical experimentation. In our case the exact order and procedure for the EIT system has been dictated by the processing software.

The hardware requirements of the EIT data acquisition system were very similar to the experiments of Polyrides (2002) and Weereld et al. (2001). The EIT system required a computer with sufficient speed and memory to acquire the data, a constant current source, and a matrix/multiplexer system to handle the switching of the applied current and voltages. The voltage data acquisition works by measuring the voltage potential at all electrodes, while applying a designated current across an opposing pair of electrodes. The system must then change the pair of electrodes applying current and remeasure the

voltage potential at all electrodes. In this experiment with 48 electrodes, 2,304 measurements were made, 48 voltage measurements per current drive pair. An example of the numbering system for the top ring is shown in Figure 2-3.

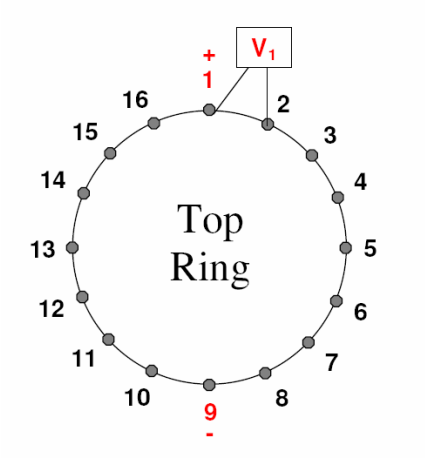

Figure 2-3: Numbering scheme for top electrode ring with current drive from electrode 1 to opposite electrode 9 and differential voltage measurement between electrode 1 and 2.

The switch matrix was arranged in a 4x64 (1-wire) configuration, meaning that 64 external channels are crossed with four internal channels, giving the ability to access 64 electrodes voltages from four input channels. This setup used 4x48 channels, 48 electrodes crossed with one current source, one ground, and two voltage measurement channels. The entire scan time for 2,304 measurements required approximately 40 seconds. This introduced the assumption that the saturation does not change significantly over the 40 second scan period.

The absolute accuracy of the data acquisition system is unknown, but some limitations and tolerances are apparent. The voltage measurements are precise to several hundredths of a volt, and can measure up to +/- 10 V. The limitations of concern deal with the switching matrix capabilities; the applied current cannot exceed 400 mA, the voltage may not exceed 30 V, and the switching rate is limited to 900 cycles/minute. These limitations were critical when test runs were designed in order to protect the equipment and obtain accurate results.

A schematic of the EIT data acquisition system is shown in Figure 2-4. The switch matrix and data acquisition (DAQ) card are controlled by an automated program developed in LABVIEW (details on automated program in Appendix B). The applied current and core saturation were set manually prior to the experiment, and the change in saturation was monitored by the scale. The data were then processed separately in the MATLAB program developed by the EIDORS project. During the calibration stage the resistivity meter was used manually to measure the real resistance along the core.

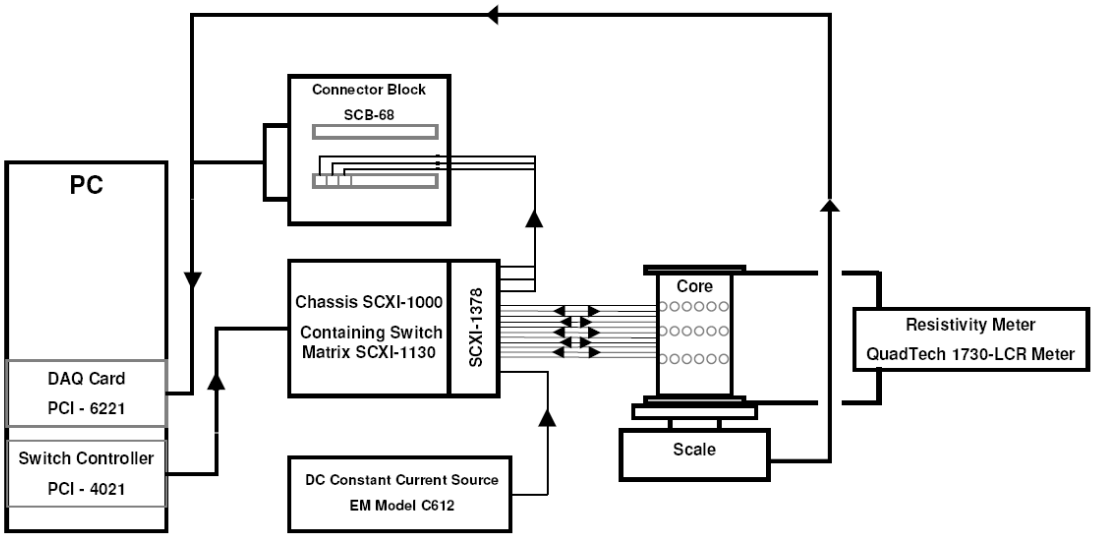

Figure 2-4: EIT system schematic. The PC cycles through the sequence by measuring the voltage potential at every electrode before changing the current source electrodes. The current is supplied by a DC current generator, while the voltage potential measurements are retrieved by the DAQ card. The scale and resistivity meter are used to calibrate the EIT measurements by providing the actual saturation and resistivity.

2.3. Data Processing

The data processing portion of EIT has been developed extensively in the medical field and this was critical to development of this experiment. The work of Polydorides (2002) was of particular importance to the project because he worked extensively in addressing the data processing issue of soft-field tomography, and eventually contributed to the development of the MATLAB toolkit called EIDORS (Electrical Impedance Tomography

and Diffuse Optical Tomography Reconstruction Software). EIDORS is a MATLAB program package developed collaboratively by EIT research groups in order to help advance the field of EIT as a whole.

The data processing portion of this experiment was accomplished with the EIDORS V3.0 toolkit. The toolkit was essential because of the challenges in solving an EIT inversion problem. The EIT inversion problem is a nonlinear, ill-posed problem that is very intensive computationally. The basis of the EIDORS package is that it utilizes a finite element model for forward calculations and a regularized nonlinear solver to obtain a unique and stable inverse solution (Polydorides et al. 2002). The package is equipped with a mesh generator, several standardized EIT methods, a graphical output, and supports two-dimensional and three-dimensional EIT systems.

The scheme utilized in our system was a forward solution with a mesh of 13,824 finite elements, and an inverse solution mesh of 1,536 elements. The program calculated the inverse solution iteratively by using a weighted image prior of the homogeneous solution.

A major change implemented in reconstructing the resistivity image was the omission of the positive and negative current electrode voltage measurements. These extreme voltages are caused by electrode skin effects (Bagotzky 1993), and were justified in their omission because we are interested in the internal resistivity distribution not the electrode resistivity. The final images reconstructed in EIDORS are shown later in section 4. These images indicate the relative resistivity to the initial resistivity assigned for the forward solution.

Chapter 3

3. Procedure

The following procedural steps were used to perform EIT on the Berea core under drainage conditions due to evaporation.

3.1. Core Saturation

Prior to saturation, the core was dried at a temperature of 50ºC under a 32 psi vacuum for 4 hrs. The drying temperature needed to be relatively low due to the plastic and solder. Upon complete drying, the complete core system was weighed to provide the zero saturation weight. The core was then placed into the vacuum cylinder as shown in Figure 3-1. This figure illustrates the initial set-up of the saturation apparatus. The water in the volumetric flask was previously deaerated prior to the experiment by imposing a vacuum on the volumetric flask for 20 minutes at 300 millitorr, after this the vacuum pump was attached as shown.

In this initial stage all components of the system were separated by closed valves. To start, the vacuum pump was turned on and allowed to create a vacuum prior to opening valves 3 and 4, which started the deaeration of the core. The dry ice heat exchanger was used to remove any moisture in the vacuum line, preventing it from reaching the pump. The vacuum pump deaerated the vacuum cylinder for 4 hrs at ~100 millitorr, effectively removing all air from the core. After this period of deaeration valves 3 and 4 were once again closed, and the pump was powered off. Now with the vacuum cylinder under vacuum, valve 2 was opened to allow water into the vacuum cylinder and for the saturation by imbibition to begin. After the core was fully submerged the three-way valve 1 was opened to atmospheric pressure to assure all entrapped air dissolved in to the water. The core was then allowed to remain submerged overnight to ensure the system came to equilibrium, and 100% saturation was achieved. After this period the core was taken out

of the vacuum cylinder, all excess water on the wires and core was quickly removed, and the core with all wires was weighed. This weight provided the 100% saturation weight, and also provided the pore fluid weight to calculate total porosity.

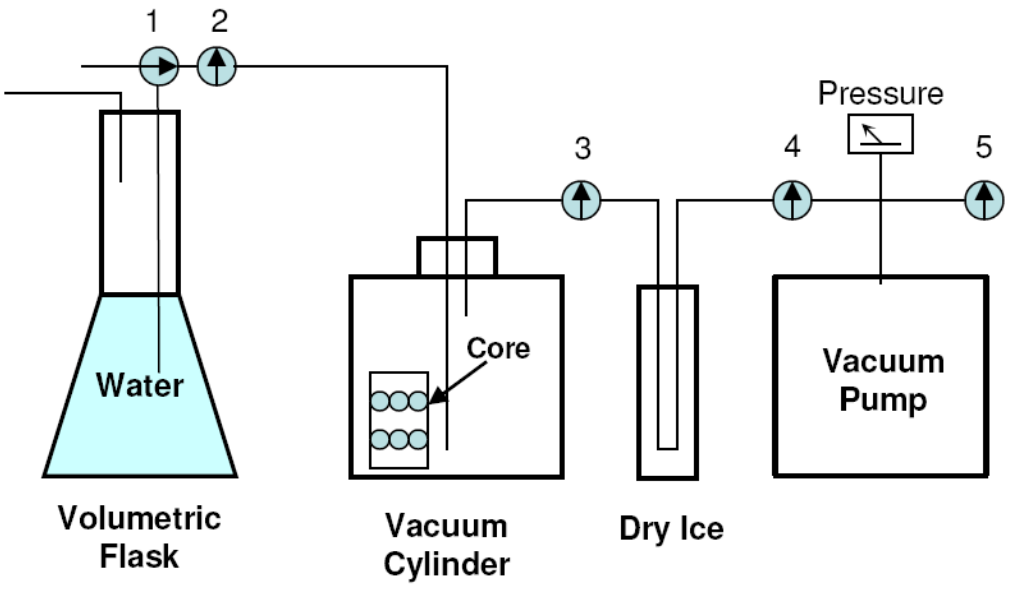

Figure 3-1: Initial set-up for core saturation. Prior to saturation water is deaerated with vacuum pump, and core is oven dried in a vacuum chamber.

3.2. Saturation Measurement

The real saturation of the core was calculated from the decrease in weight from fully saturated conditions, combined with knowing the porosity of the core and the weight of the total pore fluid. The weight was monitored using a Sartorius BP6100 balance, which transmitted the weight measurement to the LabView program upon request. Figure 3-2 is a picture of the setup during an experiment.

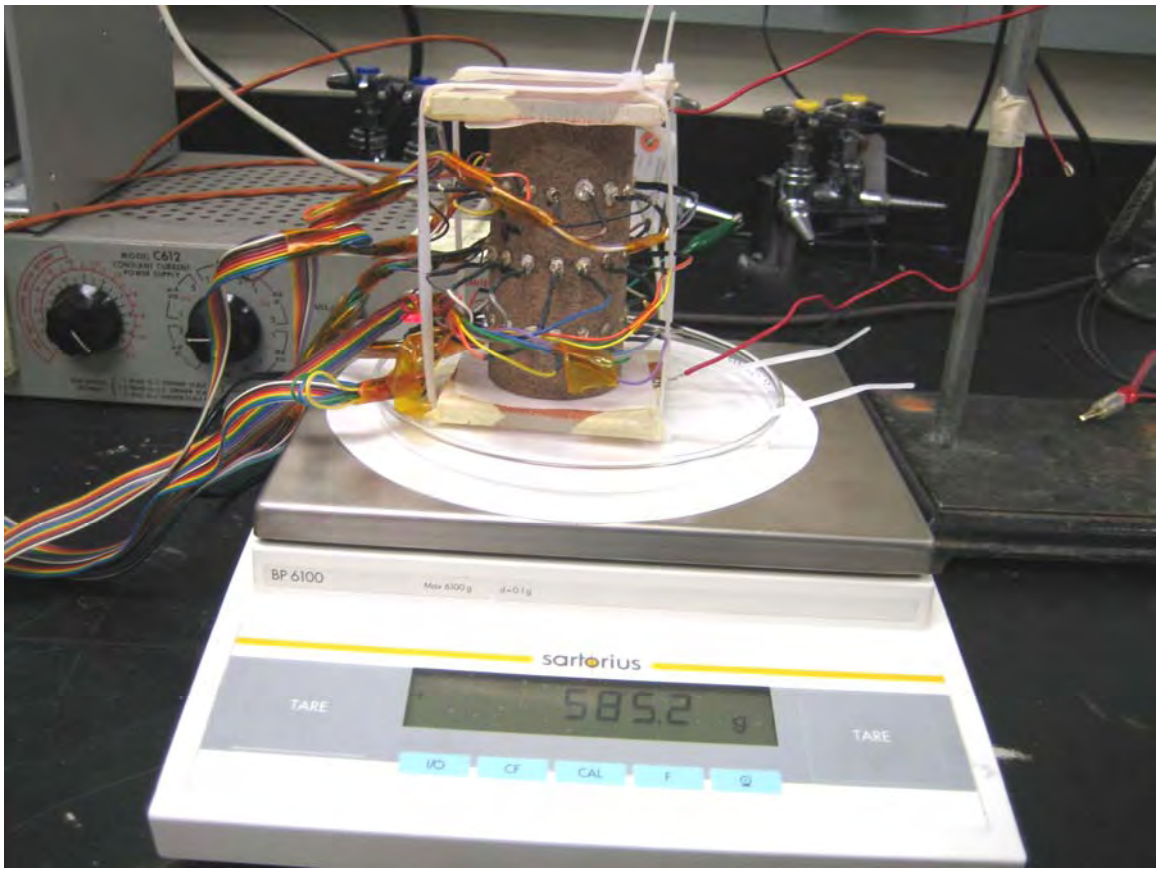

Figure 3-2: EIT experiment with Sartorius balance to monitor saturation and resistivity meter plates attached to measure the true resistance.

3.3. EIT Measurement

The automated measurement system for the experiment was developed in a LabView program. The detailed LabView program can be found in Appendix B. Outlined in Figure 3-3 is the simplified code structure for the program. First the weight of the core is recorded then the actual EIT portion begins. The EIT system works by driving a constant current across two opposing electrodes, example electrodes 1 and 9, as in Figure 2-3. Then the voltage difference is measured between electrodes 1 and 2 and stored. In the newest system, the current direction is then reversed, and again the voltage difference is measured and stored between electrodes 1 and 2. This provides the voltage difference between two electrodes for current flowing in each direction. The current drive is then reversed again back to its original state, and the voltage measurement steps to the next

electrodes, 2 and 3. After all 48 electrode pairs have been measured, the current drive steps to the next electrode current drive pair, 2 and 10. At the completion of an EIT scan there will be two voltage data sets, one normal current drive and the other reversed current drive, each containing 2304 voltage measurements. In the first few experiments the current drive was not reversed between voltage measurements, therefore only the normal current drive data set was created.

```
Storage(CoreWeight)          %%Read core weight from scale and store
For Current_Drive =1:48      %%(Example: assign + to electrode 1 – to electrode 9)
    For Voltage_Measurement = 1:48 %%(Example: Measure voltage between electrodes 1-2, 2-3, 3-4, etc.)
        StorageNormal = Measure(Voltage_Measurement)
        Flip(Current_Drive) %%Example: swap - to electrode 1 + to electrode 9, flipping current direction
        StorageReverse= Measure(Voltage_Measurement)
        Flip(Current_Drive) %%Flip back to original state
    end
end
```

Figure 3-3: Simplified code structure for EIT LabView program.

3.4. EIT Processing

The processing of the EIT voltage data was accomplished using the EIDORS toolkit for MATLAB. The complete MATLAB program utilizing the EIDORS functions is listed in Appendix A. Shown below in Figure 3-4 is a simplified code structure for the data processing. The first step in solving for the internal resistance distribution was to create a finite element model of the core and electrodes, Figure 3-5. With this finite element model and a set current, the forward problem was solved assuming a system of homogeneous resistance for the voltage data. The next step was to load the real data set and solve the inverse problem. The inverse problem was solved using the standard Polydorides method, but the EIDORS toolkit offers several other regularized nonlinear solvers to obtain a unique and stable inverse solution (Polydorides et al. 2002). After solving for the resistivity distribution the average resistivity of the core was obtained by taking the geometric mean of all the elements.

```
For 1:Number_of_EIT_scans
        Create Electrode Model      %%Create simple 48 electrode finite element model of core and electrodes
                                    with homogeneous resistance
        Solve Forward Problem       %% Solve for voltage distribution with Electrode Model
        Load (StorageNormal, StorageReverse) %%Load real voltage measurements
        Create Inverse Electrode Model %% Same as Electrode model except less finite elements
        Solve Inverse Problem       %% Solve for resistivity distribution using the Inverse Electrode Model, forward
                                    voltage measurements, and the real voltage measurements.
        StorageResistivity = Geometric Mean (Resistivity Distribution)
                                    %% Geometric mean of the calculated resistivity distribution is stored
end
```

Figure 3-4: Simplified code structure for EIDORS MATLAB data processing program.

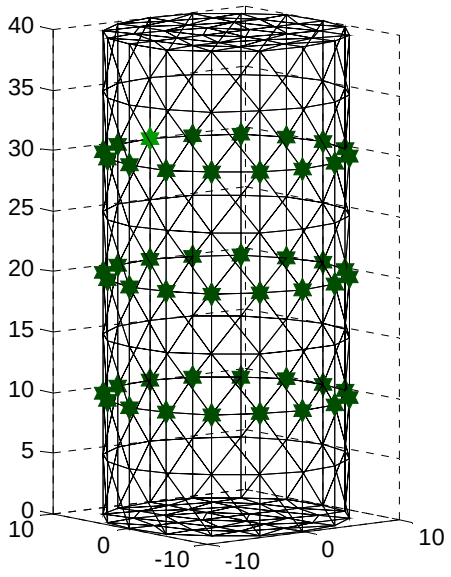

Figure 3-5: Finite Element Mesh and electrodes used to solve forward problem.

3.5. LCR Resistance Measurement

The LCR unit used was a QuadTech-1730 LCR meter, which is a standard high precision laboratory unit for measuring the resistance of materials, and has been used extensively in core studies. The LCR was used in this experiment to provide a measure of the true resistance for comparison to the EIT inferred resistance. A schematic of the setup is

shown below in Figure 3-6. The contact copper plates were placed on each end and held there by plexiglas and two nylon zip-ties (not shown). The two wire leads coming from the contact plates were then attached to a ring stand to prevent disturbance of the weight measurement during resistance measurements. Resistance measurements were made between EIT scans by attaching the LCR clamps to the contact wire leads. Measurements could not be made simultaneously with EIT scans due to short-circuiting effects. The resistance measurements were recorded at 100, 20, and 1 kHz, along with the weight of the core.

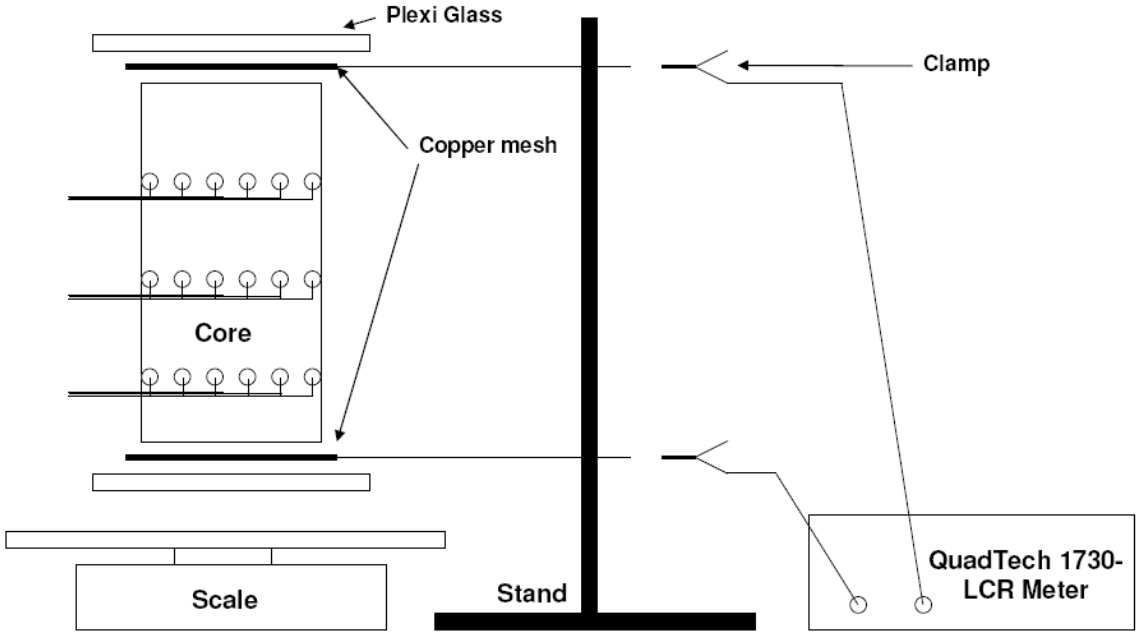

Figure 3-6: Schematic of the resistance measurement. The LCR meter was attached in between EIT scans to measure the core's end-to-end resistance.

Chapter 4

4. Results and Discussion

4.1. Qualitative Tests

After completing the assembly of the EIT apparatus qualitative tests were conducted to investigate the capabilities and limitations of the EIT system. The system was able to detect saturation changes in the core, while the changes in saturation were verified visually. The data acquisition time was approximately 40 seconds for each scan, with a post-processing reconstruction time of 74 seconds for images similar to those in Figure 4-1. If the resistance distribution did not change significantly between each scan, the image reconstruction following the first would require only approximately 2 seconds. The reason for this was the previous solution was used as an initial guess for the next data set.

The physical results that came from this initial experiment were significant for designing future experiments. A difficulty arose when working with the core at very low saturations, $S_w<10\%$. At these saturations the differential voltages between electrodes went above the measuring capability of the system. The reason for this sudden spike in voltages is believed to be that the connate water became disconnected. Therefore this problem was addressed in two ways. First the voltage measurements at the current drive electrodes were omitted because the maximum voltage measurable by the system is 10V, and because of the undesirable electrode impedance caused by skin effects. Secondly, the EIT scans were limited to imaging when the saturation was sufficient to provide proper connectivity to the electrodes. This saturation limit was about $S_w>10\%$.

Due to this saturation constraint, an initial saturation had to be present to allow imaging for the series of tests shown in Figure 4-1. Figure 4-1 (a) shows the resistivity distribution from the initial saturation that occurred by allowing distilled water to imbibe into the dry core for 3 hrs. Figures 4-1 b, c, and d show the step decreases in resistivity as the core

was submerged in ionic water to the bottom, middle, and top ring respectively and then removed for imaging. The difference in fluid resistivity is clearly apparent, but the diffusive nature of EIT prohibits the imaging of a sharp front at this time.

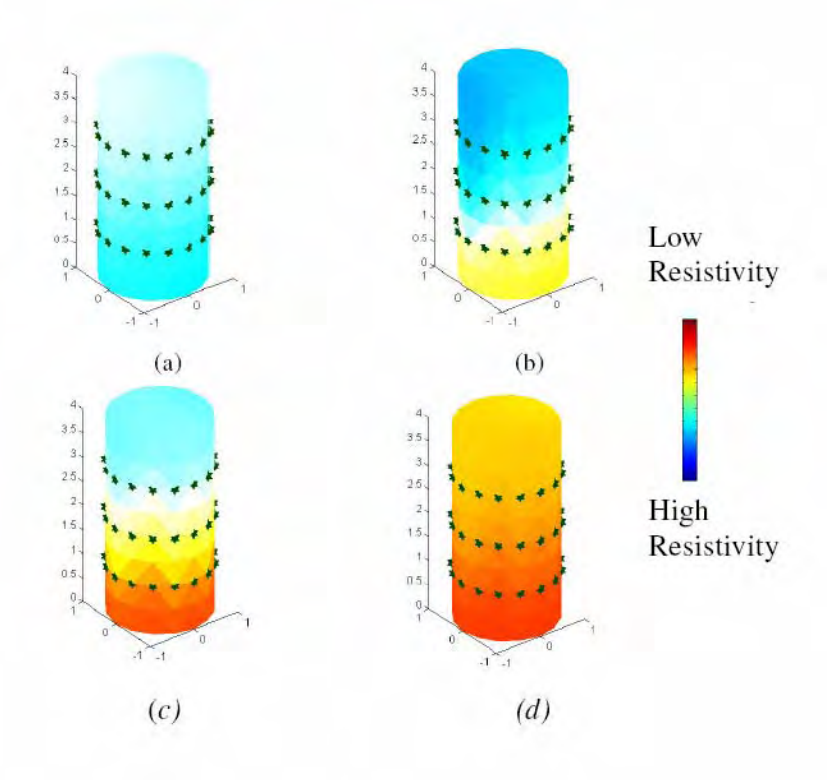

Figure 4-1: (a) Resistivity distribution after natural imbibition for 3 hrs. (b) Followed by submerging the column in water up to bottom ring. (c) Submerging to middle ring (d) Submerging to top ring.

4.2. Porosity Measurement

Each full EIT experiment provided a porosity measurement to be used for saturation calculations in partial saturation experiments. Knowing the volume of the core, the porosity measurement was calculated by measuring the weight difference between the 100% saturated and 0% saturated core. This complete drying and saturating of the core was performed six times, giving an average porosity of 25%, Table 4-1. The variation in calculated porosity can be attributed to errors in removing excess water from the wires and the surface of the core when measuring the 100% saturated weight.

Table 4-1: Porosity calculation for EIT core.

	Test Date					
	2/16	**3/8**	**4/4**	**5/4**	**5/11**	**5/22**
Dry wt (g)	494.7	494.7	495.4	495.4	498.5	496.1
Saturated wt (g)	545.4	545.0	543.8	544.5	546.9	546.2
Pore fluid wt (g)	50.7	50.3	48.4	49.1	48.4	50.1
Core Volume (cm^3)	196.3	196.3	196.3	196.3	1963	196.3
Porosity (%)	25.8	25.6	24.7	25.0	24.7	25.5

4.3. EIT Calibration

Before applying EIT to multiphase flow systems, the technique needed to be calibrated to determine the corresponding resistivity-saturation relationship. The anticipated relationship between the core saturation and the resistivity index was based upon Archie's Second Law for saturation, Equation 4-1. Here the resistivity index R_I, defined as the relative resistance between R_t, the cores resistance at a given saturation, and R at $S_w = 1$. (Mavko et al. 1998) However, this equation must be modified due to the evaporation process used in the experiment. Since the core saturation is changing by evaporation, the dissolved solid concentration is no longer a constant, but is now a function of saturation, Equation 4-2. Here C_i is the initial dissolved ion concentration at $S_w = 1$ and C_s is concentration as a function of saturation in ppm. By knowing the new concentration C_s, the new fluid resistance can be calculated with Equation 4-3, (Li and Wang 1993). Now to take into account the resistance of the fluid being a function of saturation Equation 4-1 is modified to Equation 4-4. Where $R_{f,s}$ is the fluid resistance at a concentration, and R_f is the fluid resistance at the initial concentration of $S_w = 1$ (Daily and Ramirez 2000).

$$R_I = \frac{R_s}{R} = S_w^{-n} \tag{4-1}$$

$$C_s = \frac{C_i}{S_w} \tag{4-2}$$

$$R_{f,s} = 12.676 \times e^{(-.00079 \times C_s)} + 1.2125 \quad \textbf{(4-3)}$$

$$R_I = \frac{R_s}{R} = \frac{R_{f,s}}{R_f} S_w^{-n} \quad \textbf{(4-4)}$$

The saturation of the quantitative EIT experiment was monitored by measuring the dry weight of the core, saturating the core, and then recording the cores weight before each EIT scan. In the first quantitative EIT experiment, EIT 4_06, the resistivity meter was included to provide the true resistivity measurement. The EIT scan was performed by applying a current of 2.2 μA to the core saturated with a 0.5% NaCl solution, 5,000 ppm. The true resistance was measured at three different frequencies 100 kHz, 20 kHz, and 1 kHz between scans with the LCR meter. The results of this entire experiment and Archie's law are compared in Figure 4-2. The LCR data agreed with the resistivity vs. saturation data of Roberts (2002) and the modified Archie's equation. In the EIT data a decrease in the resistivity index was observed with decreasing saturation until $S_w = 0.75$. In comparing the EIT to the resistivity meter results, it is clear that this apparent decrease in resistivity with decreasing saturation is not a physical phenomenon of the core, but is a result of the EIT system itself. This error was attributed to the movement of ions in solution due to the DC voltage; this phenomenon is further addressed in Section 4.4. However, the resistivity meter and the lower saturation EIT data do match Archie's equation fairly well.

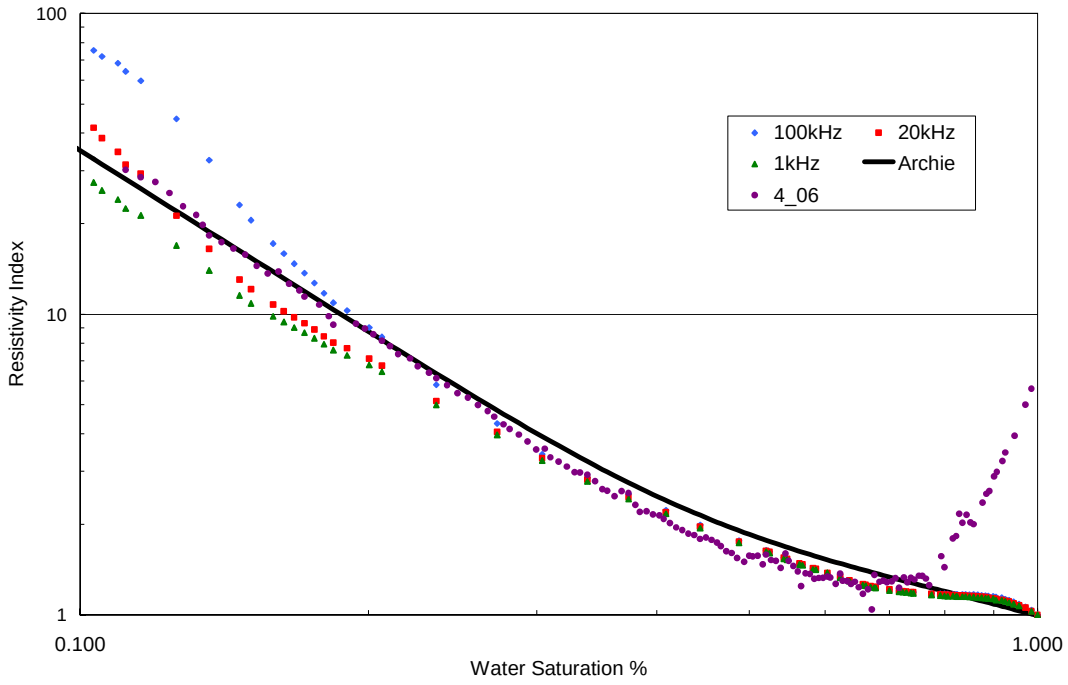

Figure 4-2: Resistivity Index vs. Saturation for run 4_06.

In the following EIT test the LabView program structure was modified in an attempt to negate the DC current effects as observed in Figure 4-2. The new code structure simply included a function to reverse the current between each voltage measurement as seen in Figure 3-3. However, due to the limitations of LabView the DC switching only achieved ~40 Hz.

To test the new AC type system the 5_11 EIT experiment was performed by applying a current of 2.2 μA, but distilled water was used in an attempt to minimize ion transport. However, dissolved solids were still present due to entrapped salt. The core saturation only reached 55% because the core was saturated by submerging the core in distilled water for 4 hrs without deairing the core or water. A comparison of the results and Archie's law is shown in Figure 4-3. The results include the regular EIT data set and the reverse data set, which is the resistance inferred by reversing the current. Here it is clear that both data sets are consistent with one another and with Archie's equation over this

saturation range. However, two key observations must be pointed out, the range in which the DC current had its greatest effect, S_w >0.75, was not tested in this run. The second observation is the first two data points of both data sets. They indicate significantly different resistivity indexes initially, but converge to the same value as time passes. This observation of differing resistances based on current direction is indicative of a polarization phenomenon (Bagotzky 1993).

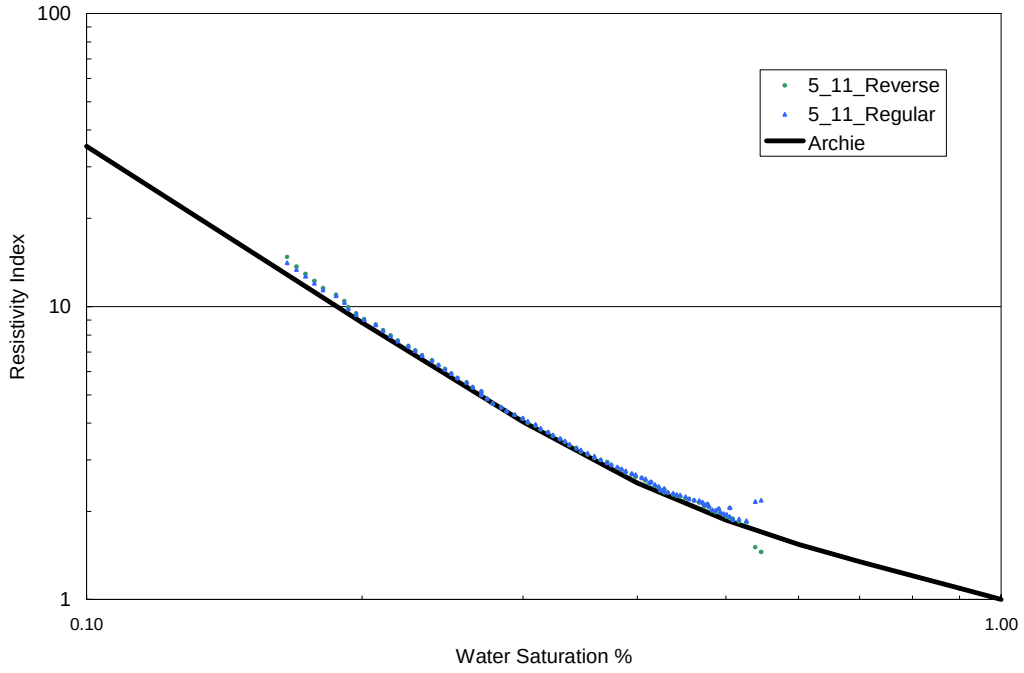

Figure 4-3: Resistivity Index vs. Saturation for run 5_11.

After the 5_11 EIT experiment, the 5_13 experiment was performed to test the DC effects at high saturations. A current of 2.2 μA was used with distilled water, and the resistivity meter was used to provide a quantitative comparison. The EIT resistivity and LCR meter results are shown in Figure 4-4 and Figure 4-5 respectively. The EIT resistivity still indicated a DC phenomenon at high saturations, with initially differing resistivity indexes, again suggesting polarization (Bagotzky 1993) This experiment indicates 40 Hz is not a high enough frequency to stop the transport of ions, but appears to have slowed

down the transport. Figure 4-6 provides a comparison between the 5_11 and 4_6 EIT experiments. It appears the ions were mobile until about S_w= 0.5 in the 5_11 experiment compared to the ions moving until S_w = 0.75 in the 4_6 experiment. One possible explanation for this is the dissolved ions did not reach the steady state position as quickly as occurred with the pure DC system alone. Essentially the voltage switching was only able to slow down the mobility of ions, not stop it.

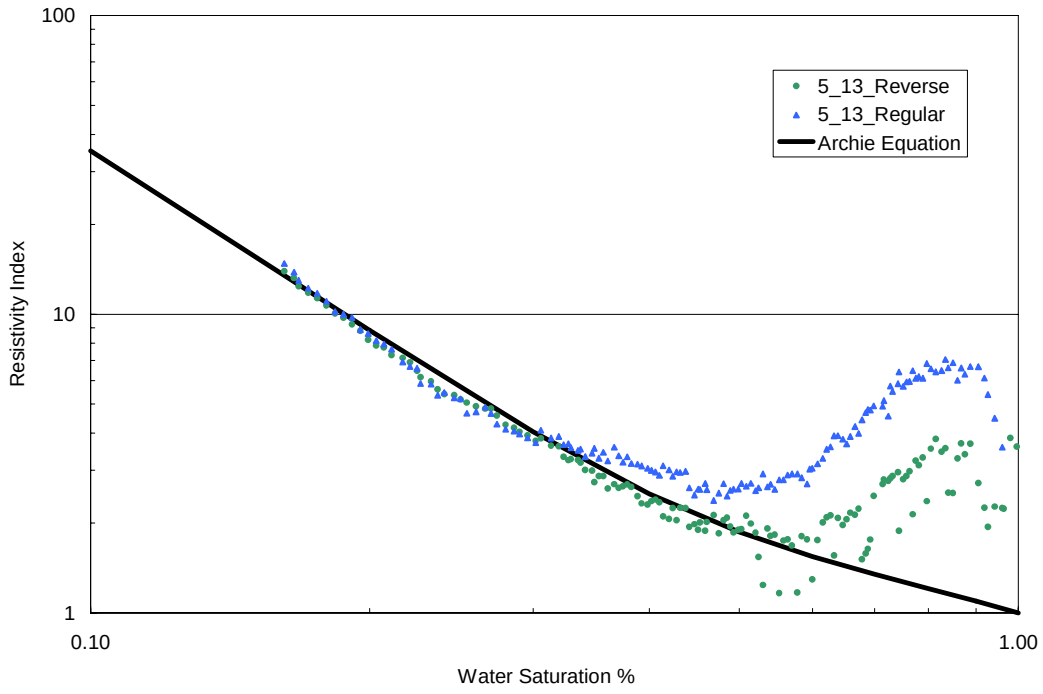

Figure 4-4: Resistivity Index vs. Saturation for run 5_13.

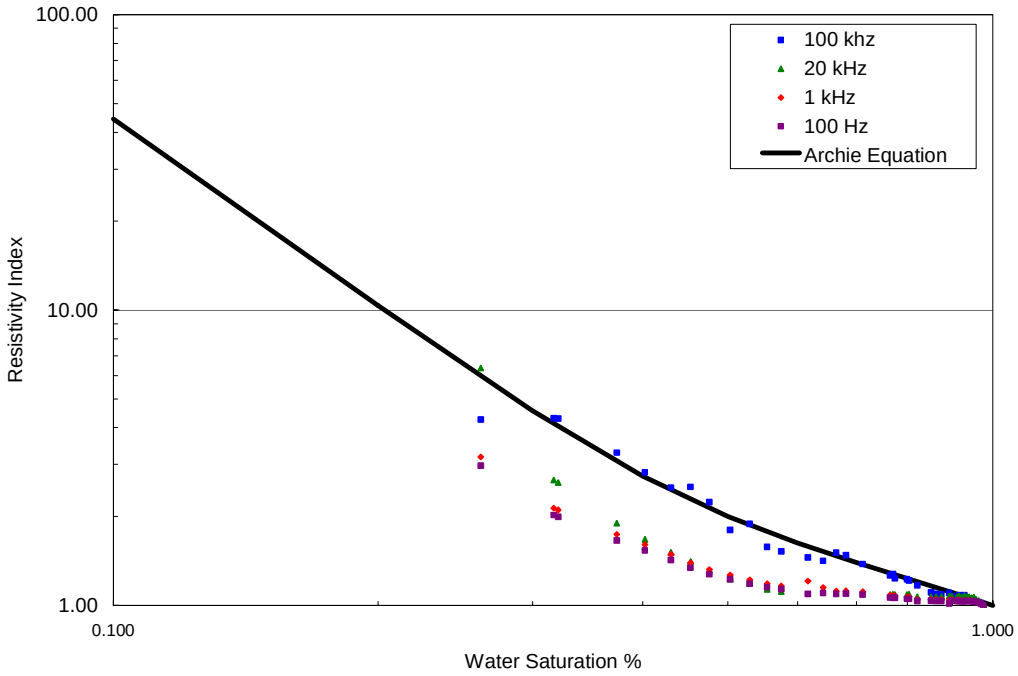

Figure 4-5: Resistivity Index vs. Saturation for run 5_13 with resistivity meter.

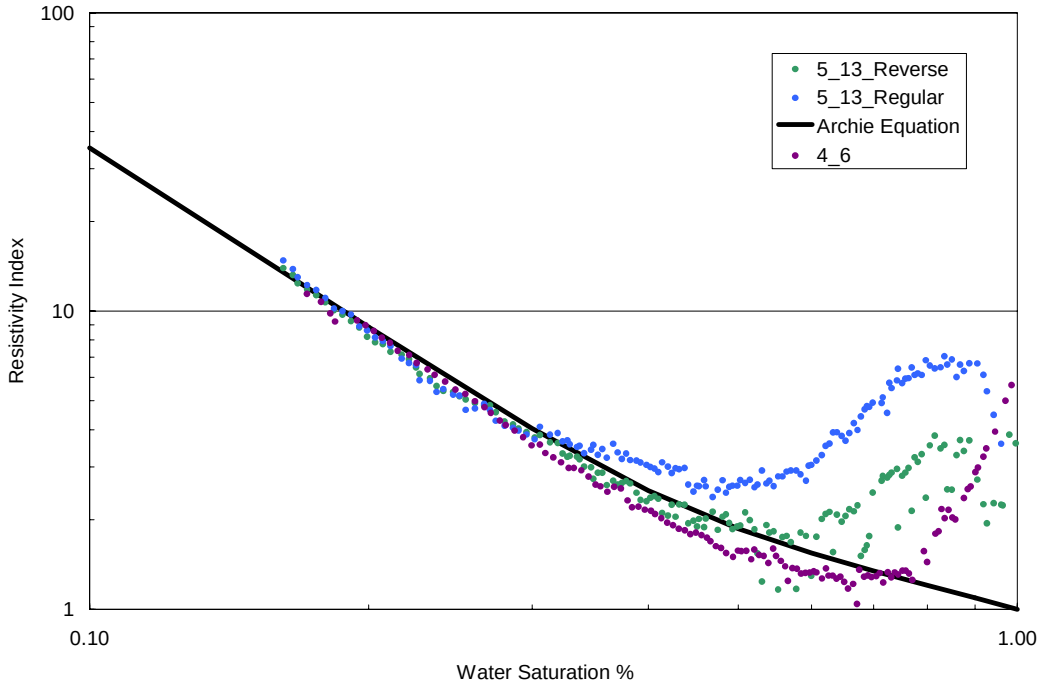

Figure 4-6: Comparison between Resistivity Index vs. Saturation for run 5_13 and run 4_6.

After test 5_13 it was apparent that the DC voltage switching could not substitute for a high frequency AC voltage source. Therefore the effect of increasing the current was tested in experiment 5_17. The experiment was performed following the same procedure as experiment 5_11, but with the current increased to 5.0 μA. The results from the experiment are shown in Figure 4-7. The data once again followed Archie's equation quite well at low saturations except for a slight deviation at the beginning of desaturation. Interestingly, it appears the first two data points exhibit polarization effects as in test 5_11. However, this time the effect appears to be larger, presumably due to the increased current. Figure 4-8 provides a comparison of the two data sets, 5_11 and 5_17. Both data sets exhibit little noise in the resistivity index measurement throughout the course of drainage, when compared to complete experiments that started at complete saturation. The reason for this is not clear at this time, but is speculated to be associated with the DC current and may also deal with the reaeration of the pore fluid during desaturation.

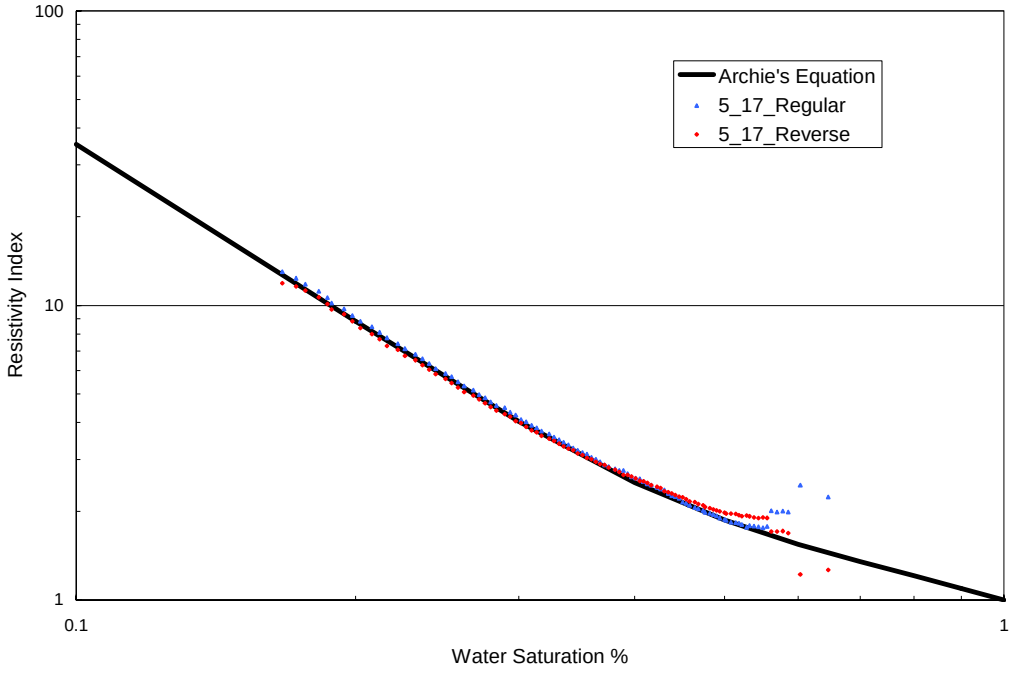

Figure 4-7: Resistivity Index vs. Saturation for run 5_17 inferred by EIT.

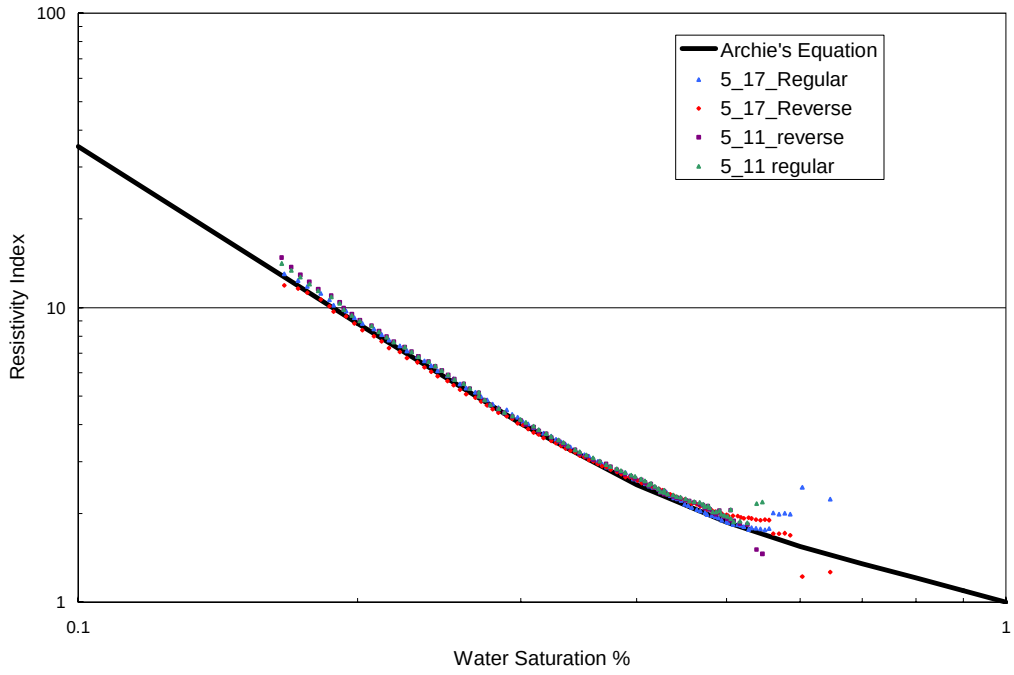

Figure 4-8 Comparison between Resistivity Index vs. Saturation for run 5_17 and run 5_11.

4.4. Effects of DC Current

It was clear in the experiments that a DC voltage source causes erroneous resistivity results at high saturations. This phenomenon has been known in electrochemistry for a period of time. In electrochemistry, solution conductivity is measured with a conductivity cell. The cell consists of a voltage applied to two flat metal plates immersed in a solution; the resulting current is measured to calculate the resistance. Typically an AC voltage is required to measure the conductivity of a solution, because the solution conductivity is affected by ion mobility. If a DC voltage source is used the ions near the electrodes mobilize toward the electrode and soon become depleted, causing polarization, and eventually decreasing the conductivity of the solution. This phenomenon is overcome by using a high frequency AC voltage source, but capacitance effects must be taken into account to measure the real conductivity (Bagotzky 1993).

4.5. Comparison to Archie's Equation

In comparing the LCR measured resistivity to Archie's equation it was clear that the modification pointed out by Daily and Ramirez (2000) was critical in capturing the physics of the system. The modification took into account the decreasing fluid resistivity caused by the evaporation process increasing the concentration of dissolved ions in solution. It was noted that with this modified equation, if the initial ion concentration is above 5000 ppm the effects of the modification are negligible. This is due to the fact that above 5000 ppm the resistivity of the solution does not decrease significantly.

Chapter 5

5. Conclusions

5.1. Applicability of EIT

The experiments conducted upon the Berea sandstone core indicate that EIT is an alternative technique for studying multiphase systems of contrasting resistivity, and the system has the capability of detecting displacement fronts in near real-time. The quantitative portion of the experiment found the technique to be capable of measuring the saturation distribution at saturations accurately between 20% < S_w < 65%. The lower limitation was imposed due to the requirement of a connate water connection to all electrodes. The higher limitation was set due to ion mobility effects caused by the DC voltage source. It is anticipated that the EIT system will be able to measure saturations accurately up to S_w= 100% with the proper implementation of an AC voltage source.

5.2. Specific Conclusions from the EIT System

The diffusive nature of the EIT process currently makes the reliable detection of sharp saturation fronts difficult, but not necessarily impossible. It is anticipated that with continuing advancements in inversion procedures, image resolution will increase.

- EIT scans were limited to imaging when the saturation was sufficient to provide proper connectivity to the electrodes. This roughly corresponds to Sw>20%.
- It appears the ions were mobile until about S_w= 0.5 in the 5_11 experiment compared to the ions moving until S_w = 0.75 in the 4_6 experiment.
- The resistivity meter and the lower saturation EIT data match Archie's equation quite well.

- Changing the core saturation by evaporation affected the fluid resistivity significantly. The evaporation caused the dissolved solid concentration to become a function of saturation, requiring the modification of Archie's equation.

- In comparing the LCR measured resistivity to Archie's equation it was clear that the modification pointed out by Daily and Ramirez (2000) was critical in capturing the physics of the system.

- With the DC reversal system it appeared the ions were mobile until about S_w= 0.5 compared with mobility until S_w=0.75 for a one-way DC current alone. One possible explanation for this is the dissolved ions did not reach the steady state position as quickly as occurred with the pure DC system alone. Essentially the DC switching was only able to slow down the mobility of ions, not stop it.

- An average porosity of 25% was measured for the Berea sandstone core.

- Increased polarization effects were observed at the first two data points between test 5_11 and test 5_17 due to an increase in the applied current.

- Both test 5_11 and test 5_17 exhibited little noise in the resistivity index measurement throughout the course of drainage, when compared to complete experiments that started at complete saturation. The reason for this is not clear at this time, but is speculated to be associated with the DC current and may also be influenced by the reaeration of the pore fluid.

Chapter 6

6. Future Work

The next step in the development of the EIT technique is finishing the saturation-resistivity calibration, because this is required before any quantitative experiments can be performed in regards to geothermal systems. With the implementation of an AC voltage source it is believed the system will be able to measure the saturation accurately up to 100% without the fluid resistivity changing due to the current. The AC current source currently of interest is the Keithley Model 6221 AC and DC current source. This unit is a wide-band ultralow current unit that meets the specifications required for EIT (Bragos et al. 1994). Upon the successful calibration of mean saturation and resistance, the saturation distribution inferred with EIT may be compared to the distribution measured by a traditional X-Ray CT scan.

In the future, with the uncertainties and limitations of the system understood, the technique may be applied in several areas at varying scales. In the laboratory, EIT may be applied to geothermal cores at reservoir pressures and temperatures to understand the pore scale physics within a geothermal reservoir. At the reservoir scale, a future possibility is to investigate the development of an in-situ EIT system, where boiling fronts may be monitored, residual saturation determined, and reinjection systems investigated.

Nomenclature

V = voltage

i = current

σ = electric impedance

ϕ = electric potential

ϖ = frequency

ε = electric permittivity

References

Bagotzky, V.S., 1993, Fundamentals of Electrochemistry, Plenum Publishers, New York.

Belen, R.P., Jr.. and Horne, R.N., 2000 "Inferring In-Situ and Immobile Water Saturations from Field Measurements", Geothermal Resources Council Transactions 24

Bragos, R., Rosell, J., and Riu, P., 1994, “A Wide-Band AC-Coupled Current Source for Electrical Impedance Tomography” Physiol. Meas. Vol. 15 (1994), A91-A99

Daily, W., and Ramirez, A., 2000, “Electrical Resistance Tomography”, Final Report 200 East Vadose Test Site Hanford Washington.

Li, K. and Wang, J., 1993, "Experimental Investigation on the relationship between resistivity and water saturation in low permeability rock with low salinity," internal report, RIPED, CNPC.

Mavko, G., T. Mukerji, and J. Dvorkin, 1998, The Rock Physics Handbook: Cambridge University Press.

Molinari, M., 2003, “High Fidelity Imaging in Electrical Impedance Tomography”, Ph.D. dissertation, University of Southampton, Southampton, United Kingdom.

Polydorides, N., 2002, “Image Reconstruction Algorithms for Soft-Field Tomography”, Ph.D. dissertation, University of Manchester, Manchester, United Kingdom.

Polydorides, N., and Lionheart W.R.B., 2002, “A MATLAB Toolkit for Three-dimensional Electrical Impedance Tomography: a Contribution to the Electrical Impedance and Diffuse Optical Reconstruction Software Project”, Meas. Sci. Technol. 13 No 12 December 1871-1883.

van Weereld, J.J.A., Player M.A., Collie, D.A.L, Watkins, A.P., and Olsen, D., 2001, “Flow Imaging in Core Samples by Electrical Impedance Tomography”, SCA Society of Core Analysts.

Roberts, J.J., 2002, “Electrical Properties of Microporous Rock as a Function of Saturation and Temperature”, Journal of Applied Physics, Vol. 91, No. 3

Roberts, J.J., Abelardo, R., Carlson, S., William, R., Bonner, B.P., and Daily, W., 2001 “Laboratory and Field Measurements of Electrical Resistivity to Determine Saturation and Detect Fractures in a Heated Rock Mass” Geothermal Resources Council Transactions 25

Singha, K., and Gorelick, S. M., 2005, “Saline tracer visualized with three-dimensional electrical Field-scale spatial moment analysis”, Water Resour. Res., 41, W05023, doi:10.1029/2004WR003460.

Appendix A

A. Electrical Impedance Tomography MATLAB Code

```
%%%%%%%%%%%%%%%%%%%%%%%%%%%%%%%%%%%%%%%%%%%%%%%%%%%%%%%%%%%%%%%%%%%%%%%
%% Robert Stacey
%% All non-standard MatLab functions can be downloaded
%% from EIDORS eidors3d.sourceforge.net
%% 6/1/06
%% Electrical Impedance Tomography Inversion Code


clc
close all
clear all

for k = 1:158  %%Number of EIT scans performed

    %%%%%% Step 1 %%%%%%%%%%%%%%%%%%%%%%%%%%%%
    % Create 48 electrode 3D Model
    %%%%%%%%%%%%%%%%%%%%%%%%%%%%%%%%%%%%%%%%%%%
    I = .0022;              %%%Current applied during experiment
    n_elec    = 16;         %Number of eletrodes per ring
    e_levels  =[7 5 3];     %Ring number for electrodes
    elec_spec = {'planes', n_elec,e_levels};     %Set up electrode planes
    n_rings   = 3;                               %Number of electrode rings
    options   = {'no_meas_current','no_rotate_meas'};
    %Did you measure current electrodes?
    %Did you rotate measurments with current electrodes?
    Levels    = [0,2,4,6,8,10,12,14,16]/4; %height of planes for FE mesh

    Mesh_rings= 4;   %Number of rings out from center when creating mesh

    params = mk_circ_tank(Mesh_rings, Levels, elec_spec); %%Create mesh
    params.nodes = params.nodes*10;                 %%change scale here
    %% Create stimution pattern same as experiment
    params.stimulation = mk_stim_patterns(n_elec,n_rings,'{op}','{ad}',options,I);
    %% How should you solve the forward problem?
    params.solve     = 'aa_fwd_solve';
    %% How should you solve the calculate the system matrix?
    params.system_mat= 'aa_calc_system_mat';
    %% Bundle everything in a structural array called fwd_model
    mdl_3d           = eidors_obj('fwd_model',params);

    %%Show the 3D finite element model with electrodes
     show_fem(mdl_3d);
     axis equal
     pause
```

```
    %%%%%%%%%%%%%%%%%%%%%%%%%%%% Extract Homogeneous data%%%%%%%%%%%%%%%%%
    mat = ones(size(mdl_3d.elems,1),1); %% check the 10^-2
    homg_img = eidors_obj('image','homogeneous image', 'elem_data',mat,'fwd_model',↵
mdl_3d);
    homg_data= fwd_solve(homg_img);


    %%%%%%%%%%%%%%%%%%%%%%%%%%%%%%%%%%%%%%%%%%%%%%%%%%%%%%%%%%%%%%%%%%%%%%%%%%%%

    %%%%%% Step 2 %%%%%%%%%%%%%%%%%%%%%%%%%%%%
    % Load real data
    %%%%%%%%%%%%%%%%%%%%%%%%%%%%%%%%%%%%%%%%%%

    %%%% Creat structure for inhomogeneous data
    inh_img  = eidors_obj('image', 'inhomogeneous image','elem_data', mat,'fwd_model',
mdl_3d );
    inh_data =fwd_solve( inh_img);

    %%%% Load real data from tabdiliminated excel file, previously loaded
    load  EITData4_6_06_FINAL    %Real Data
    %% Data is the EIT data to be used in this iteration
    Data = EITData4_6_06_FINAL((1+(k-1)*2304):(k*2304));
    %% Data2 is the EIT scan Data will be compared to give relative
    %% resistance
    Data2 = EITData4_6_06_FINAL((1+(3-1)*2304):(3*2304));

    %%This portion removes all voltage measurements that use current drive
    %%electrodes
    load RemoveCurrent;
    Data(RemoveCurrent)=nan;
    Data2(RemoveCurrent)=nan;
    Data = Data(~isnan(Data));
    Data2 = Data2(~isnan(Data2));

    inh_data.meas = Data; %%This is the EIT scan you are interested in
    homg_data.meas = Data2;%% This is the scan you are comparing to



    %%%%%% Step 3 %%%%%%%%%%%%%%%%%%%%%%%%%%%%
    % Solve inverse problem (much is the same as the forward problem)
    %%%%%%%%%%%%%%%%%%%%%%%%%%%%%%%%%%%%%%%%%%
    Mesh_rings2 = 4;
    params = mk_circ_tank(Mesh_rings2, Levels,elec_spec);
    params.stimulation= mk_stim_patterns(n_elec,n_rings,'{op}','{ad}',options,I);
    params.solve =      'np_fwd_solve'; %%np solver is the fastest inverse
    params.system_mat = 'np_calc_system_mat';
    params.jacobian =   'np_calc_jacobian';
    params.misc.perm_sym='{n}';
    fm3d = eidors_obj('fwd_model', params);

    inv3d.name= 'EIT inverse: 3D';
    inv3d.solve='np_inv_solve';
    inv3d.hyperparameter.value = 1e-4; %%weight on homomeneous image prior
    inv3d.image_prior.func= 'laplace_image_prior';
    inv3d.reconst_type= 'difference';
    inv3d.fwd_model = fm3d;
    inv3d = eidors_obj('inv_model', inv3d); %%bundle into structural array
```

```
    img3 = inv_solve(inv3d,inh_data,homg_data); %% SOLVE INVERSE PROBLEM
    img3.name = '3D inverse solution';


    meanresgeo(k) = geomean(img3.elem_data; %%Geometric mean resistance
    meanres(k) = mean(img3.elem_data);      %%Arithmatic mean resistance

         show_fem(img3,[0 0]);              %%Show core with resistivity

        figure
       levels = [inf,inf,1; inf,inf,2; inf,inf,3;inf,.5,inf;]
       show_slices(img3,levels,[60]); %% Take and show slices thru the core
       pause(.25)
       close all

end
```

Appendix B

B. LabView program

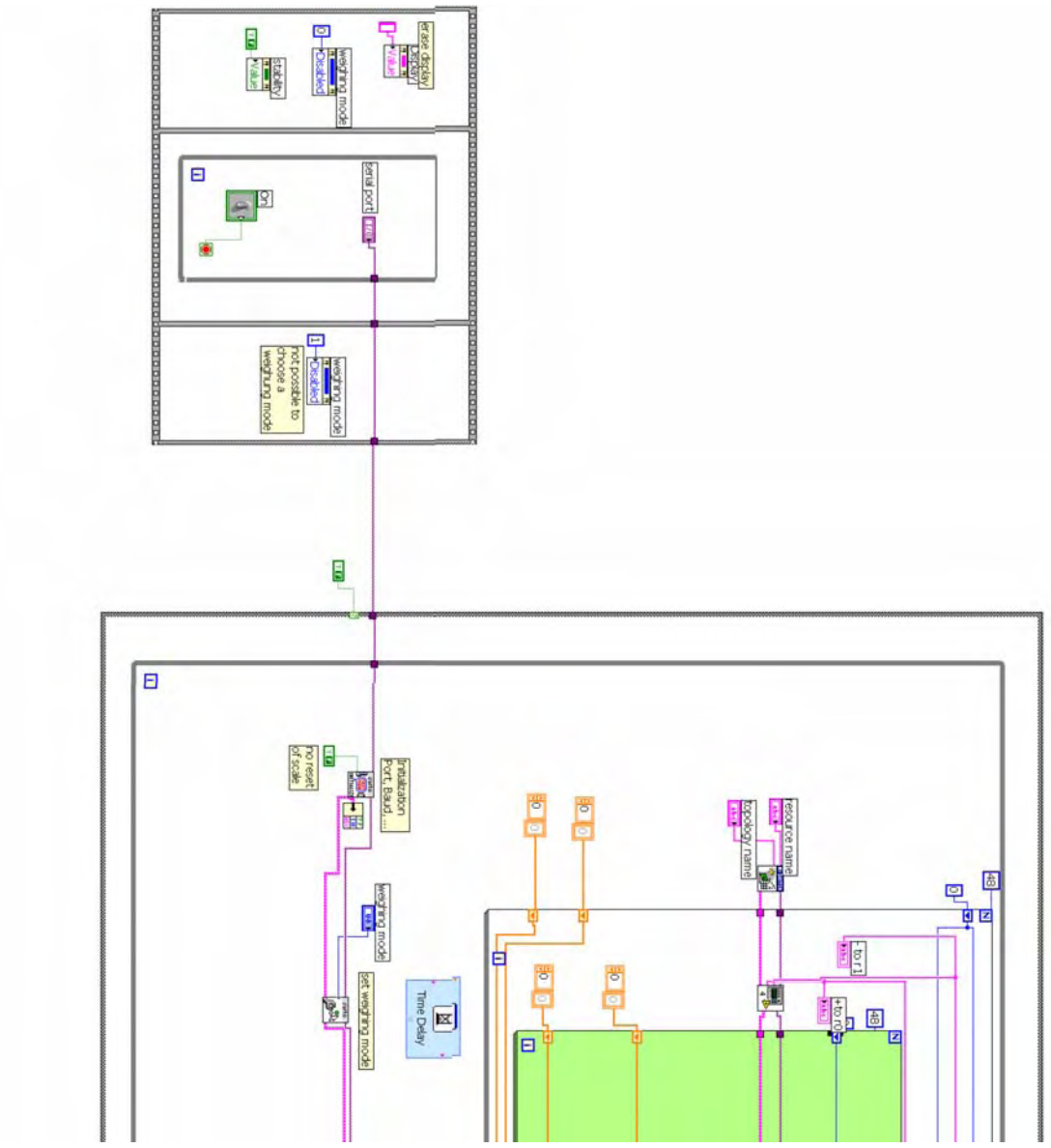

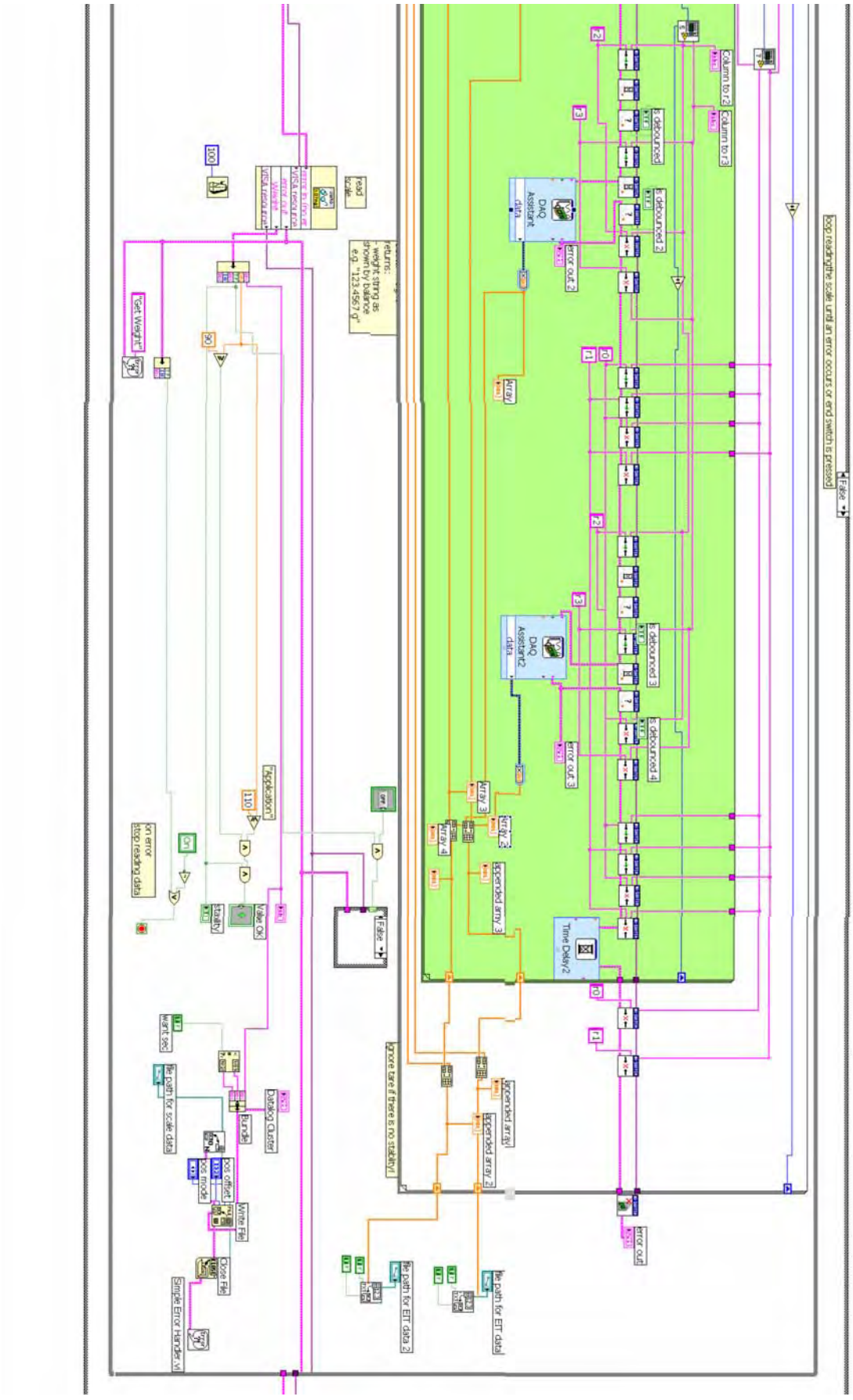
loop reading the scale until an error occurs or end switch is pressed
False
DAQ Assistant
DAQ Assistant2
error out 2
error out 3
Time Delay2
Column to r2
Column to r3
s debounced
s debounced 2
s debounced 3
s debounced 4
Array
Array 2
Array 3
Array 4
appended array
appended array 2
appended array 3
error out
"Get Weight"
read scale
returns: weight string as shown by balance e.g. 123.4567 g"
"application"
Value OK
Stability
On error stop reading data
ignore tare if there is no stability!
Weight Data
file path for scale data
Datalog Cluster
Bundle
Write File
Close File
Simple Error Handler.vi
file path for EIT data 2
file path for EIT data1

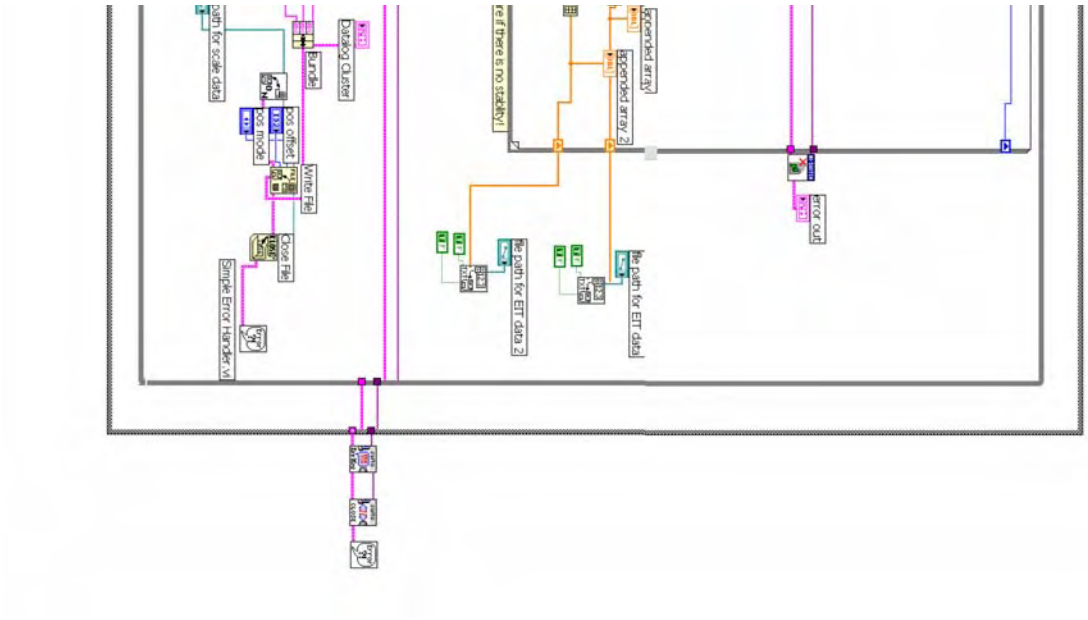
path for scale data
Bundle
Datalog Cluster
pos offset
pos incr
Write File
Close File
Simple Error Handler.vi
e if there is no stacktyp
appended array
appended array 2
error out
file path for EIT data 2
file path for EIT data1

Appendix C

C. Data Acquisition Components

Data Acquisition System

PC Hardware Components

PCI-6221 DAQ card
PCI-4021 Switch Matrix Controller

NI Components

SCXI-1000 Chassis
SCXI-1130 Switch Matrix
SCXI-1378 Matrix connection Block
SHC68-68-EP cable
SCB-68 Voltage measurements
SCXI-1349 adapter assembly

Current Source

Electronic Measurements Model C612 DC generator

Balance

Sartorius BP 6100

LCR Meter

QuadTech 1730